

---

# Quantum Efficiency and Noise-Equivalent Power of Nanostructured, NbN, Single-Photon Detectors in the Wavelength Range from Visible to Infrared

## Introduction

Single-photon-detection schemes based on sensitive and ultrafast optical quantum detectors gain their dominance in various single-photonics applications. The development of superconducting single-photon detectors (SSPD's), based on ultrathin, submicron-width NbN structures has already been reported.<sup>1-4</sup> SSPD's are ultrafast and sensitive for ultraviolet, visible, and infrared (IR) photons. They exhibit very low dark counts and require no active or passive quenching. As recently demonstrated, SSPD's exhibit real-time counting rates of above 2 GHz and a <20-ps timing jitter.<sup>5,6</sup> The SSPD operation principle has been introduced within a phenomenological hot-electron photoresponse model.<sup>1,7</sup> In this article, the results of our research on the latest generation of SSPD's are presented, including their quantum efficiency (QE) and the noise-equivalent power (NEP) in the wavelength range between 0.5 and 5.6  $\mu\text{m}$ , and their dependencies on an operating temperature in the 2.0- to 4.2-K range. The main emphasis is on the very low-temperature (2.0-K) performance of our SSPD's.

## Device Fabrication

NbN superconducting films used for the fabrication of SSPD's had a thickness of 4.0 nm and were deposited on sapphire substrates by dc reactive magnetron sputtering in an Ar and N<sub>2</sub> gas mixture. The films were characterized by a surface resistance  $R_S = 500 \Omega/\text{square}$ , a critical temperature  $T_c = 10$  to 11 K, a superconducting transition width  $\Delta T_c \sim 0.3$  K, and a critical current density  $j_c = 6$  to  $7 \times 10^6 \text{ A}/\text{cm}^2$  at 4.2 K. During our deposition process, the sapphire substrate with *c*-cut crystalline orientation was heated up to 900°C, leading to an epitaxial growth of the NbN thin film. Our detectors had a meander-type geometry that covered a  $10 \times 10\text{-}\mu\text{m}^2$  area and had a filling factor (the ratio of the area occupied by the superconducting meander to the device nominal area) of up to 0.5. The width of the superconducting stripe was typically 100 to 120 nm, but it could be as low as 80 nm. The devices were fabricated using the process based on direct electron-beam lithography and reactive ion etching.

A detailed description of our technological operations was presented in a recent publication.<sup>8</sup> During the electron-beam lithography process, the areas under which the superconductor was removed were exposed in the resist. The minimal width of the superconducting stripe did not depend directly on the electron-beam diameter; rather, it was largely determined by the electron scattering in the photoresist. The resist PMMA 950 K was used and later removed from the superconductor using the reactive ion-etching process. The choice of the 80-nm resist thickness ensured a reliable protection of the superconducting film. Significant reductions of resist thickness allowed us to fabricate meanders with a filling factor of up to 0.5 and superconducting stripes as narrow as 80 nm (Fig. 101.53).

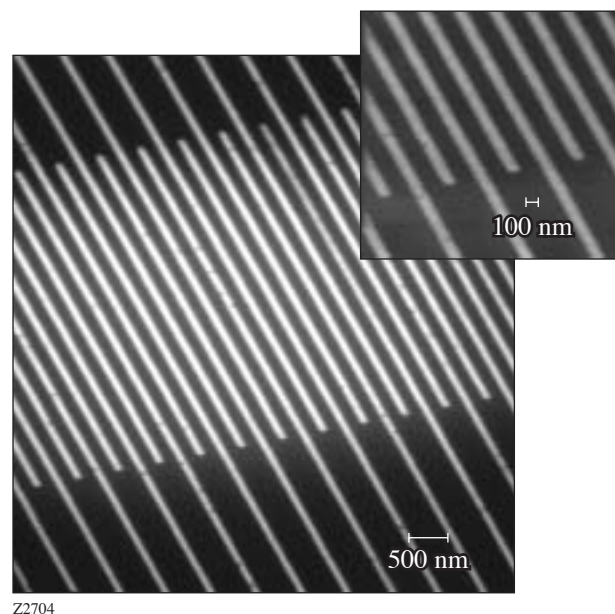


Figure 101.53 SEM (scanning electron microscope) image of an SSPD (NbN is black). The inset shows the meander structure in detail.

To test the impact of the NbN film processing on its superconducting properties, the temperature dependence of the resistance of the patterned SSPD was measured and compared to the original NbN film. The  $T_c$  and  $\Delta T_c$  of the reactive ion-etched devices and the original films were practically the same within 0.1-K accuracy. This latter fact proves the optimal character of our technological process since no negative impact on the NbN SSPD was observed. In addition, it confirmed the very high quality of our initial, ultrathin NbN films.

**Experimental Setup**

A schematic diagram of our experimental setup is shown in Fig. 101.54. The SSPD was wire-bonded to a coplanar transmission line and then connected to a very stable, constant-voltage bias source and the output circuitry through a coaxial cryogenic bias-tee. The constant-voltage operation regime ensured a rapid return to the superconducting state after the photon detection of the SSPD and prevented self-heating of the device. The entire assembly was placed on a cold plate, inside an optical cryostat. The SSPD voltage response was amplified by a room-temperature, 40-dB-gain, 1- to 2-GHz-bandwidth amplifier and then fed to a pulse counter for statistical analysis.

Light sources consisted of a set of continuous-wave (cw) laser diodes covering the range from 0.56  $\mu\text{m}$  to 1.55  $\mu\text{m}$  and pulsed laser diodes delivering 40- to 60-ps-wide pulses at a repetition rate of 1 to 103 kHz at 637-nm, 845-nm, and 1554-nm wavelengths. A grating monochromator for generating IR (1- to 5.6- $\mu\text{m}$ -wavelength) radiation was also used.

Photons from the lasers were delivered to the detector either by propagating in free space or by an optical fiber. In each case, the input radiation was focused and attenuated down to the picowatt power level or below. Sapphire input windows were used for measurements in the 0.6- to 3.0- $\mu\text{m}$ -wavelength range and silicon windows for measurements in the 1.2- to 5.6- $\mu\text{m}$ -wavelength range. Cold sapphire or silicon filters were placed inside the cryostat to cut parasitic room-temperature background radiation.

**Experimental Results and Discussion**

QE is defined as the ratio of the detection events registered by the counter  $N_{\text{reg}}$  to the number of incident photons  $N_{\text{inc}}$  for a given time interval per the device area:

$$QE = N_{\text{reg}} / N_{\text{inc}} \cdot \tag{1}$$

In cw measurements, the  $N_{\text{inc}}$  value was determined from the power incident on the device’s nominal active area of 100  $\mu\text{m}^2$  measured by a power meter. The power of our laser sources was always measured separately by calibrated optical attenuators. In experiments with pulsed sources, experimental QE was simply the probability of photon counting, measured at the one-photon-per-pulse level, incident upon the SSPD nominal area and expressed in percent.

Figure 101.55 shows that our most recent advances in SSPD fabrication technology led to the greatly improved stripe uniformity and resulted in significant QE enhancement.

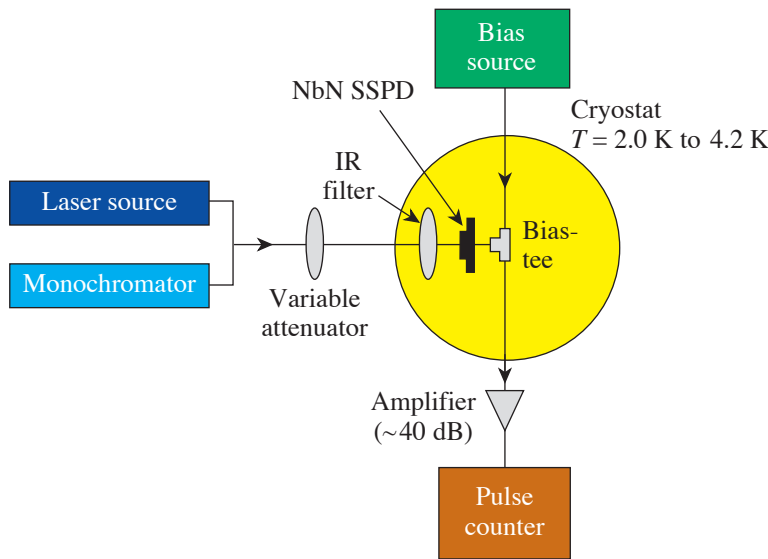


Figure 101.54  
Experimental setup.

Z2582a

Figure 101.55 presents the QE's dependence on normalized bias current  $I_b/I_c$  at two different operating temperatures. At 4.2 K, QE for visible-light photons reaches an ~30% value. One can also note in Fig. 101.55 an evidence of QE saturation at the 0.56- $\mu\text{m}$  wavelength at 4.2 K. The saturation-like behavior is, however, more obvious looking at the 2-K, 0.56- $\mu\text{m}$  data. Furthermore, for visible light, the decrease in operating temperature below 4.2 K led to no improvement in QE; therefore, the observed saturation means that in the visible range, our SSPD detects every photon absorbed by the superconducting NbN film.

From an application point of view, the telecommunication 1.3- $\mu\text{m}$  and 1.55- $\mu\text{m}$  wavelengths are the most interesting. The QE at these wavelengths at 2 K is also presented in Fig. 101.55. One can see that at 1.3  $\mu\text{m}$ , the QE reaches 30% saturation value, while at 1.55  $\mu\text{m}$ , the maximum QE is 17%. At 4.2 K, the QE for IR light is quite far from saturation. For example, the maximum QE at 1.55  $\mu\text{m}$  at 4.2 K is only 3.7% and only for  $I_b$  approaching  $I_c$  (Fig. 101.55).

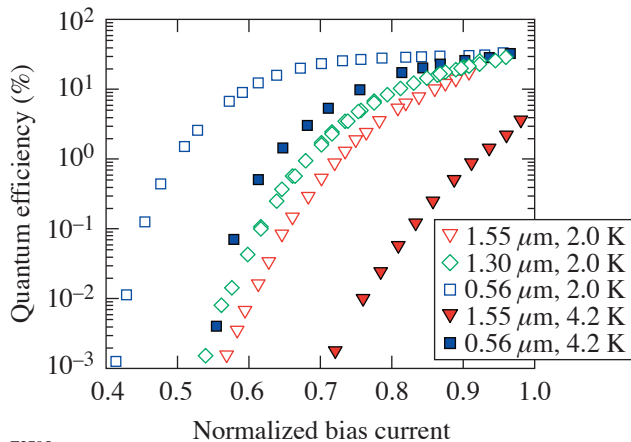


Figure 101.55  
Quantum efficiency measured at different wavelengths at 4.2-K and 2.0-K operating temperatures.

Figure 101.56 presents the dark-count rate  $R$  versus  $I_b/I_c$ .  $R$  is determined as a number of spurious counts per second when the SSPD input is completely blocked by a cold metal shield inside the cryostat. Without the shield or cold filter, e.g., when the device was directly connected to the fiber, the SSPD was exposed to 300-K background radiation, which manifested itself as extrinsic dark counts. The  $R(I_b)$  dependence

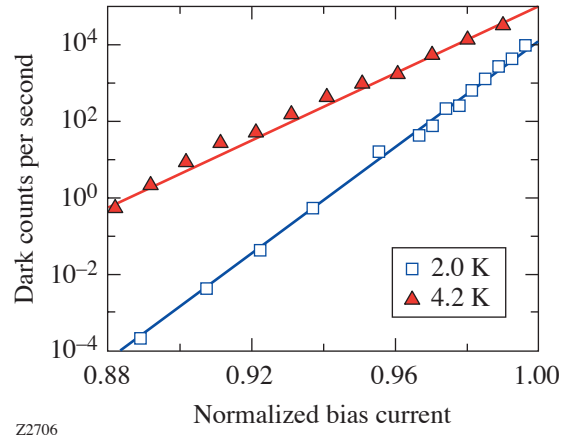


Figure 101.56  
SSPD dark counts as a function of the normalized bias current measured at 4.2 K and 2.0 K.

demonstrates the activation law in the whole biasing range used in our experiments ( $0.87 < I_b/I_c < 0.99$ ):

$$R = a \times \exp\left(b \frac{I_b}{I_c}\right), \quad (2)$$

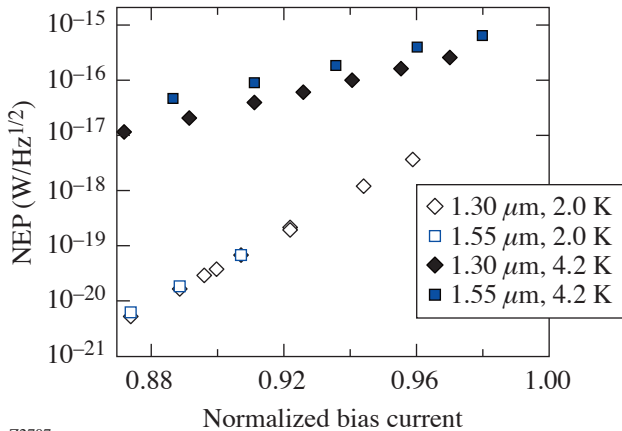
where  $a$  and  $b$  are constants. The activation-type behavior of  $R(I_b)$  extends up to over seven orders of magnitude. The minimum measured  $R$  was as low as  $2 \times 10^{-4} \text{ s}^{-1}$  and was limited by the duration of the experiment, i.e., accumulating several dark counts took about 8 h.

An optimal operation regime of the SSPD is a trade-off between QE and  $R$ . The maximum value of QE corresponds to rather high ( $\sim 1000 \text{ s}^{-1}$  or above)  $R$ . Quantitatively this interplay between QE and  $R$  can be presented in terms of the noise-equivalent power (NEP), which can be defined for quantum detectors as

$$\text{NEP} = \frac{h\nu}{\text{QE}} \sqrt{2R}, \quad (3)$$

where  $h\nu$  is photon energy. The open symbols in Fig. 101.57 show the results of the NEP calculation using Eq. (3) and experimentally measured QE (Fig. 101.55) at 1.3  $\mu\text{m}$  and 1.55  $\mu\text{m}$  and  $R$  (Fig. 101.56) values. Only the lowest points at 2.0 K (for  $I_b/I_c < 0.88$ ) were calculated using extrapolated values of  $R$ .

As one can see, at 2.0 K for photons at the telecommunication wavelengths, our SSPD's exhibit QE > 10% and simultaneously reach an NEP level as low as  $5 \times 10^{-21}$  W/Hz<sup>1/2</sup>. To our knowledge, this is the best performance for any currently available single-photon detector.



Z2707

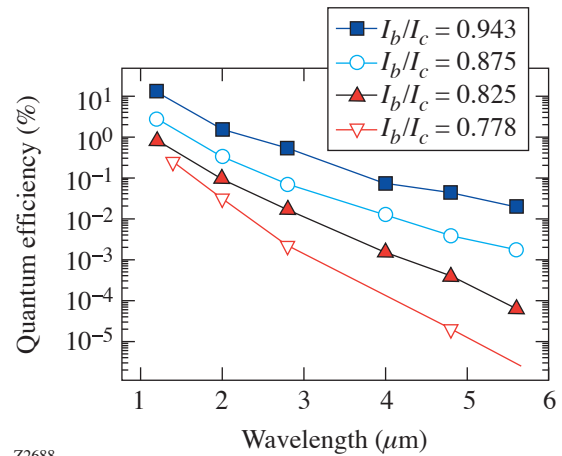
Figure 101.57

The SSPD NEP at 4.2 K (closed symbols) and 2.0 K (open symbols), calculated for 1.30  $\mu\text{m}$  (diamonds) and 1.55  $\mu\text{m}$  (squares) using the experimental  $R$  and QE values from Figs. 101.55 and 101.56, respectively.

The spectral characteristics of the NbN SSPD's using radiation from the monochromator (see Fig. 101.54) have been investigated in the IR 0.9- to 5.6- $\mu\text{m}$ -wavelength range at different operating temperatures (2.9 to 4.3 K) and bias currents. In our best devices, single-photon counting was observed up to 5.6- $\mu\text{m}$  wavelength. Figure 101.58 shows that the spectral sensitivity has exponential character and strongly depends on  $I_b$ . The highest detection probabilities are measured for  $I_b$  values very close to  $I_c$ . The decrease in operating temperature for a given  $I_b/I_c$  improves QE and also extends the SSPD's single-photon-counting capabilities farther into the IR wavelength range.

## Conclusions

The performance of our latest-generation SSPD's tested at 2.0 K has been presented. The very low-temperature operation extends the single-photon-counting capabilities of our detectors to 5.6- $\mu\text{m}$  IR wavelength. Simultaneously, at 2 K, the QE of our devices reached  $\sim 30\%$  saturation, which corresponds to the photon absorption in a 4-nm-thick NbN film. Finally, the 2-K temperature environment resulted in a drastic (over two orders of magnitude as compared to the 4.2-K opera-



Z2688

Figure 101.58

QE spectral dependencies, measured for a NbN SSPD at 3 K at different bias currents ( $I_c = 29.7$  at 3 K). Solid lines are guides for the eye.

tion) decrease in the detector dark counts. The QE increase and the  $R$  decrease led to NEP values at 2 K as low as  $5 \times 10^{-21}$  W/Hz<sup>1/2</sup> at the IR wavelength.

The demonstrated SSPD performance at 2 K shows that in the IR range, the SSPD's significantly outperform the best semiconductor devices and photomultiplier tubes. The SSPD's have already found practical applications for the debugging of very large-scale, integrated Si complementary metal-oxide-semiconductor circuits,<sup>9</sup> and they are of great interest in other areas, such as single-molecule fluorescence and high-resolution astronomy.

For applications in the areas of fiber-based and fiberless (free-space) optical quantum communications, quantum metrology, quantum key distribution, and linear optical quantum computation, it is interesting to compare the NbN SSPD with its superconducting counterparts. The other superconducting radiation detectors,<sup>10</sup> such as superconducting tunnel junctions (STJ)<sup>11</sup> and superconducting transition edge sensors (STES),<sup>12</sup> exhibit a very slow (kHz-range) photoresponse speed, and their jitter in the photon-counting mode is difficult to determine. The fundamental reason for the slow speed of these detectors is that they are bolometric (thermometer-like) devices based on superconductors with very low (below 1 K)  $T_c$ , which is dictated by the desire to reach the lowest-possible intrinsic noise levels and NEP; therefore, STJ's and STES's are not optimal for very high-speed quantum communication. The

STES's, however, are photon-number-resolving devices with very high (>80%) QE values, which makes them very attractive for quantum metrology and optical quantum computations.<sup>13</sup>

#### ACKNOWLEDGMENT

This work was funded by RFBR grant 03-02-17697 (Moscow), CRDF grant RE2-2529-MO-03 (Moscow and Rochester), and US AFOSR grant FA9550-04-1-0123 (Rochester). Additional support was provided by a MIT Lincoln Laboratory grant.

#### REFERENCES

1. G. N. Gol'tsman, O. Okunev, G. Chulkova, A. Lipatov, A. Semenov, K. Smirnov, B. Voronov, A. Dzardanov, C. Williams, and R. Sobolewski, *Appl. Phys. Lett.* **79**, 705 (2001).
2. A. Verevkin, J. Zhang, R. Sobolewski, A. Lipatov, O. Okunev, G. Chulkova, A. Korneev, K. Smirnov, G. N. Gol'tsman, and A. Semenov, *Appl. Phys. Lett.* **80**, 4687 (2002).
3. R. Sobolewski, A. Verevkin, G. N. Gol'tsman, A. Lipatov, and K. Wilsher, *IEEE Trans. Appl. Supercond.* **13**, 1151 (2003).
4. J. Zhang, W. Slysz, A. Verevkin, O. Okunev, G. Chulkova, A. Korneev, A. Lipatov, G. N. Gol'tsman, and R. Sobolewski, *IEEE Trans. Appl. Supercond.* **13**, 180 (2003).
5. A. Verevkin, A. Pearlman, W. Slysz, J. Zhang, M. Currie, A. Korneev, G. Chulkova, O. Okunev, P. Kouminov, K. Smirnov, B. Voronov, G. N. Gol'tsman, and R. Sobolewski, *J. Mod. Opt.* **51**, 1447 (2004).
6. A. Korneev, P. Kouminov, V. Matvienko, G. Chulkova, K. Smirnov, B. Voronov, G. N. Gol'tsman, M. Currie, W. Lo, K. Wilsher, J. Zhang, W. Slysz, A. Pearlman, A. Verevkin, and R. Sobolewski, *Appl. Phys. Lett.* **84**, 5338 (2004).
7. A. D. Semenov, G. N. Gol'tsman, and A. A. Korneev, *Physica C* **351**, 349 (2001).
8. G. N. Gol'tsman, K. Smirnov, P. Kouminov, B. Voronov, N. Kaurova, V. Drakinsky, J. Zhang, A. Verevkin, and R. Sobolewski, *IEEE Trans. Appl. Supercond.* **13**, 192 (2003).
9. J. Zhang, N. Boiadjeva, G. Chulkova, H. Deslandes, G. N. Gol'tsman, A. Korneev, P. Kouminov, M. Leibowitz, W. Lo, R. Malinsky, O. Okunev, A. Pearlman, W. SByz, K. Smirnov, C. Tsao, A. Verevkin, B. Voronov, K. Wilsher, and R. Sobolewski, *Electron. Lett.* **39**, 1086 (2003).
10. A. D. Semenov, G. N. Gol'tsman, and R. Sobolewski, *Supercond. Sci. Technol.* **15**, R1 (2002).
11. J. H. J. de Bruijne *et al.*, *Opt. Eng.* **41**, 1158 (2002).
12. B. Cabrera *et al.*, *Appl. Phys. Lett.* **73**, 735 (1998).
13. A. J. Miller *et al.*, *Appl. Phys. Lett.* **83**, 791 (2003).

